

Theory of edge states in a quantum anomalous Hall insulator/ spin-singlet *s*-wave superconductor hybrid system

Akihiro Ii¹, Keiji Yada², Masatoshi Sato³, and Yukio Tanaka¹

¹ *Department of Applied Physics,*

Nagoya University,

Nagoya, 464-8603, Japan

² *Venture Business Laboratory,*

Nagoya University,

Nagoya, 464-8603, Japan

³ *Institute for Solid State Physics,*

University of Tokyo,

Kashiwanoha 5-1-5, Kashiwa,

Chiba 277-8581, Japan

(Dated: April 10, 2019)

Abstract

We study the edge states for a quantum anomalous Hall system (QAHS) coupled with a spin-singlet *s*-wave superconductor through the proximity effect, and clarify the topological nature of them. When we consider a superconducting pair potential induced in the QAHS, there appear topological phases with nonzero Chern numbers, *i.e.*, $\mathcal{N} = 1$ and $\mathcal{N} = 2$, where Andreev bound states appear as chiral Majorana edge modes. We calculate the energy spectrum of the edge modes and the resulting local density of states. It is found that the degenerate chiral Majorana edge modes for $\mathcal{N} = 2$ are lifted off by applying Zeeman magnetic field along the parallel to the interface or the shift of the chemical potential by doping. The degeneracy of the chiral Majorana edge modes and its lifting are explained by two different winding numbers defined at the time-reversal invariant point of the edge momentum.

I. INTRODUCTION

Andreev bound state (ABS) has been one of the central issue in superconductivity and condensed matter physics. It has been established that ABS is generated at the edge of unconventional superconductor where pair potential changes sign on the Fermi surface [1–5]. ABS realized in spin-triplet chiral p -wave superconductor has remarkable properties since the ABS has a linear dispersion around $k_y = 0$, where k_y is a momentum parallel to the surface [6, 7]. The time reversal symmetry is broken and spontaneous charge current is induced along the edge [7]. Nowadays, this ABS has been recognized as a chiral Majorana edge mode [8]. It is an analogous state to the chiral edge mode of Quantum Hall system (QHS) [9]. In QHS and its analogous superconducting state, the bulk edge correspondence has been discussed based on the Chern number which is one of the topological numbers in condensed matter physics [10].

It has been found recently that gapped time-reversal invariant systems also can support gapless edge states. In HgTe/CdTe quantum well, helical edge modes is generated due to the strong spin-orbit coupling. This system is so called Quantum spin Hall system (QSHS) [11, 12]. There are also analogous systems in the world of superconductivity. In non-centrosymmetric (NCS) superconductors[13, 14], where the spin-orbit coupling is important as in the case of QSHS, the presence of helical Majorana edge modes has been predicted [8, 15, 16]. The helical Majorana edge mode is a special ABSs which is expressed by two counter moving chiral Majorana fermions [8]. Instead of charge current, spin current is spontaneously generated along the edge. Several new features of spin transport stemming from these helical Majorana edge modes have been predicted [15–19]. Furthermore, it has been clarified there are several types of helical Majorana edge modes with [15–19] and without dispersion in NCS superconductors [20–23]. As well as chiral p -wave superconductors, the gapless edge modes in NCS superconductors can be characterized by the bulk topological numbers.

In general, superconducting states with topologically protected edge states are dubbed as topological superconductor [8, 24, 25] and the classification of topological superconductors has been done [25]. In particular, chiral Majorana edge modes have been a hot issue in the context of topological quantum computing. However, chiral Majorana edge mode generated in the chiral p -wave pair potential is fragile against impurity scattering. And the transition temperature of chiral p -wave superconductor Sr_2RuO_4 [26] is rather low. Thus, chiral

Majorana edge mode generated from simple spin-singlet s -wave superconductors is highly desired [27, 28]. It has been proposed that a chiral Majorana edge mode is produced at the interface of ferromagnet/spin-singlet s -wave superconductor junction on the substrate of three-dimensional topological insulator (TI) [27]. Also, a simpler scheme using the Rashba spin-orbit interaction and the Zeeman field has been proposed [28]. The essential point is the simultaneous presence of the broken inversion symmetry by the strong spin-orbit coupling and the time reversal symmetry breaking by ferromagnet or the Zeeman field.

In this paper, we investigate one more other way to realize chiral Majorana edge modes by using the chiral edge state of QHS attached with spin-singlet s -wave pair potential. Since the external magnetic field is very strong, it is difficult to induce pair potential for an ordinary QHS. However, as Qi *et.al.* has proposed [29], this difficulty is overcome by considering a quantum anomalous Hall system (QAHS), instead of QHS, where the exchange field is not so strong. QAHS can be realized by the doping of magnetic impurity in QSHS [30, 31]. In this scheme, the presence of the chiral Majorana edge modes can be controlled by the band mass term m , chemical potential μ and the pair potential Δ . The number of chiral Majorana edge modes can be classified by using the Chern number \mathcal{N} [8].

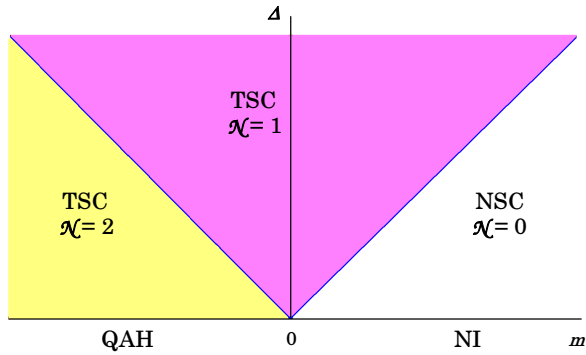


FIG. 1: (Color online) Schematic illustration of the phase diagram of the QAH+SC hybrid system for $\mu=0$, proposed by Qi, Hughes and Zhang [8]. The x axis denotes the mass term m and the y axis denotes the magnitude of the superconducting pair potential Δ . $\mathcal{N} = 2$ and $\mathcal{N} = 1$ phases with $\Delta \neq 0$ are topological superconductor (TSC). $\mathcal{N} = 0$ phase is non topological superconductor (NSC). If $\Delta=0$, the present system changes from QAH state to normal insulator (NI). For nonzero Δ , the energy gap of the bulk closes at two boundaries of the phase diagram.

In the following, we study the edge states for a QAHS coupled with a spin-singlet s -wave

superconductor through the proximity effect, and clarify the topological nature of chiral Majorana edge modes. We calculate the energy spectrum of the edge state and the resulting local density of states for various Chern number \mathcal{N} . To clarify the difference between the $\mathcal{N} = 1$ and $\mathcal{N} = 2$ state, we apply Zeeman magnetic field. We find that when the direction of the magnetic field is parallel to the interface, the degeneracy of the two chiral Majorana edge modes in $\mathcal{N} = 2$ states are lifted off. In order to understand the topological nature in detail, we evaluate the winding number of the bulk Hamiltonian. This number corresponds to the number of the zero energy state due to the presence of the bulk edge correspondence. We also clarify that the degeneracy of chiral Majorana edge modes in $\mathcal{N} = 2$ can be lifted off by shift of chemical potential from zero.

The organization of the paper is as follows. In Sec. II, we introduce the model of QAHS with spin-singlet s -wave superconductor. In Sec. III A, we calculate the energy dispersion of the edge state and the corresponding local density of state at $\mu = 0$ with and without Zeeman magnetic field. In Sec. III B, we introduce the winding number at $k_y = 0$ in order to study the topological property of above edge states. In Sec. III C, we calculate the energy dispersion of the edge state for $\mu \neq 0$. In Sec. IV, we summarize the results.

II. FORMULATION

We take a simple QAHS in the two-dimensional square lattice model, which is obtained by the replacement $p_{x,y} \rightarrow \sin p_{x,y}$ and $p_x^2 + p_y^2 \rightarrow 4 - 2(\cos p_x + \cos p_y)$ in the model used in [29]. The Hamiltonian describing low energy excitations of the quasiparticle is

$$\mathcal{H}_{QAH} = \sum_{\mathbf{p}} \psi_{\mathbf{p}}^\dagger h_{QAH}(\mathbf{p}) \psi_{\mathbf{p}} , \quad (1)$$

$$\begin{aligned} h_{QAH} &= \mathbf{d}(\mathbf{p}) \cdot \boldsymbol{\sigma} \\ &= \begin{pmatrix} m(\mathbf{p}) & A(\sin p_x - i \sin p_y) \\ A(\sin p_x + i \sin p_y) & -m(\mathbf{p}) \end{pmatrix} \end{aligned} \quad (2)$$

with

$$\psi_{\mathbf{p}} = \begin{pmatrix} c_{\mathbf{p}\uparrow} \\ c_{\mathbf{p}\downarrow} \end{pmatrix} \quad (3)$$

where $\mathbf{d}(\mathbf{p}) = (A \sin p_x, A \sin p_y, m(\mathbf{p}))$, $\boldsymbol{\sigma}$ is Pauli matrix, and $m(\mathbf{p}) = m + B(4 - 2(\cos p_x + \cos p_y))$. The band mass term $m(\mathbf{p})$ determines the magnitude of energy shift of up and down

spin. A , B and m are material parameters. The sign of m changes the topological property of the system. Here note that the presence of B term is crucial to create a QAHS. The energy dispersion of the above Hamiltonian is symmetric for the mass term m for $B = 0$, but is asymmetric for $B \neq 0$. In other words, a nonzero value of B makes the sign of m meaningful. We take $A=B=1$ in our following calculation.

In the following, we consider the proximity effect by an attached spin-singlet s -wave superconductor, where pair potential is induced in the QAHS. The system is described by the BdG Hamiltonian,

$$\mathcal{H}_{BdG} = \frac{1}{2} \sum_{\mathbf{p}} \Psi_{\mathbf{p}}^\dagger \begin{pmatrix} h_{QAH}(\mathbf{p}) - \mu & \hat{\Delta} \\ \hat{\Delta}^\dagger & -h_{QAH}^*(-\mathbf{p}) + \mu \end{pmatrix} \Psi_{\mathbf{p}} \quad (4)$$

with

$$\hat{\Delta} = \begin{pmatrix} 0 & \Delta \\ -\Delta & 0 \end{pmatrix}, \quad \Psi_{\mathbf{p}} = \begin{pmatrix} c_{\mathbf{p}\uparrow} \\ c_{\mathbf{p}\downarrow} \\ c_{-\mathbf{p}\uparrow}^\dagger \\ c_{-\mathbf{p}\downarrow}^\dagger \end{pmatrix} \quad (5)$$

where μ is the chemical potential, Δ the induced pair potential of the spin-singlet s -wave superconductor.

In order to calculate the local density of states (LDOS) at the edge, we introduce infinite potential along the y -axis as shown in Fig. 2. We calculate the Green function at $x = 1$ by t -matrix formulation [33]. The system is infinite for the y -direction while it is semi-infinite for the x -direction (See Fig. 2). Since translational invariance is absent along the x -direction, only the momentum k_y along the y -direction is a good quantum number. We express the Green functions by using spatial coordinate x and x' for fixed k_y as follows;

$$\begin{aligned} \hat{G}(x, x', k_y, \omega) &= \hat{G}_0(x, x', k_y, \omega) \\ &- \hat{G}_0(x, 0, k_y, \omega) \frac{1}{\hat{G}_0(0, 0, k_y, \omega)} \hat{G}_0(0, x', k_y, \omega) \end{aligned} \quad (6)$$

with

$$\hat{G}_0(x, x', k_y, \omega) = \frac{1}{N_x} \sum_{k_x} e^{ik_x(x-x')} \hat{G}_0(k_x, k_y, \omega), \quad (7)$$

$$\hat{G}_0(k_x, k_y, \omega) = \frac{1}{\omega - \mathcal{H}(k_x, k_y)} \quad (8)$$

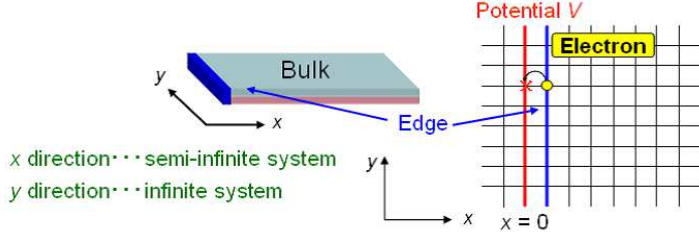


FIG. 2: (Color online) Schematic illustration of QAHS with spin-singlet s -wave superconductor in 2D system. A red line denotes the infinite potential barrier and a blue line denotes the edge. In the actual calculation, the x -direction of the system is restricted finite width with N_x ($N_x = 4096$). We have checked that the finite size effect is negligible. We use periodic boundary condition along the y -direction.

where N_x is a total number of lattice points for the x -direction. In the right hand side of Eq.(6), the first term denotes the unperturbed bulk Green function, and the second term is the scattering effect at the edge. The momentum resolved LDOS at the edge $x = 1$ $N(k_y, \omega)$ is written as

$$N(k_y, \omega) = -\frac{1}{\pi} \left(\text{Im}[\hat{G}_{11}^R(x, x, k_y, \omega)] + \text{Im}[\hat{G}_{22}^R(x, x, k_y, \omega)] \right) \Big|_{x=1} \quad (9)$$

where the upper suffix R means retarded Green function; replacing ω to $\omega + i\delta$ with infinitesimal positive number δ , and the lower indices 11 and 22 indicate the matrix elements. And we obtain the LDOS at the edge for energy ω measured from the Fermi level as follows

$$D(\omega) = \frac{1}{N_y} \sum_{k_y} N(k_y, \omega) \quad (10)$$

where N_y is a total number of lattice points for the y -direction. We set $N_x = N_y = 4096$ in the actual calculations. In the next section, we will show the spectrum $N(k_y, \omega)$ and $D(\omega)$.

III. RESULTS

A. edge states for $\mu = 0$

We first show the momentum resolved LDOS at the edge $N(k_y, \omega)$. The magnitude of the bulk energy gap E_g is given by the minimum value of $|m + \Delta|$ and $|m - \Delta|$. We

fix $\Delta = 0.25$ and $\mu = 0$. We change the value of m for (a) $m = -0.5$, (b) $m = 0$, and (c) $m = 0.5$ corresponding to $\mathcal{N} = 2$, $\mathcal{N} = 1$ and $\mathcal{N} = 0$ phases, respectively. In every case, E_g is 0.25 [29]. The bright line between upper and lower bands corresponds to the chiral Majorana edge modes for $-0.25 < \omega < 0.25$. On the other hand, the background structure with parabolic shape of the spectrum with $|\omega| > 0.25$ expresses the continuum level originating from energy bands of the bulk QAHS. We can see the chiral Majorana

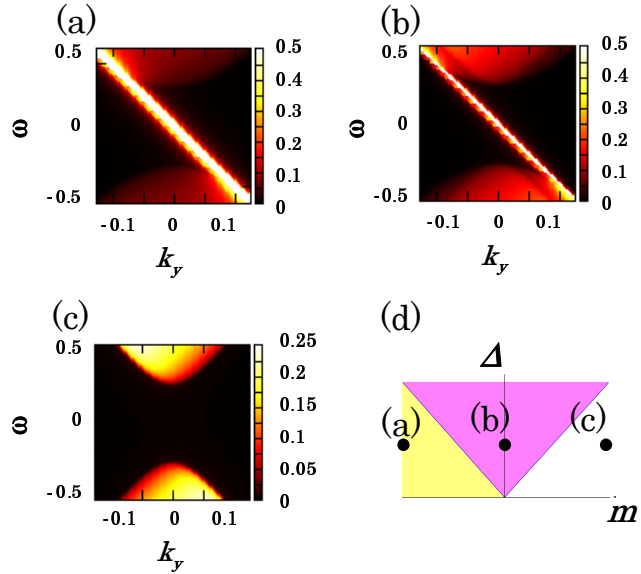


FIG. 3: Momentum resolved LDOS at the edge $N(k_y, \omega)$ is plotted as a function of ω and k_y for $\Delta = 0.25$. (a): $m=-0.5$, (b): $m=0$, and (c): $m=0.5$; these three cases are shown on m - Δ space in (d), where (a), (b) and (c) belong to $\mathcal{N} = 2$, $\mathcal{N} = 1$ and $\mathcal{N} = 0$ case, respectively. (d)Schematic phase diagram for $\mu = 0$.

edge modes for (a) and (b), but no edge mode in (c) as expected by the Chern number [29].

It is interesting to look at LDOS at the edge $D(\omega)$ since it can be observed by scanning tunneling spectroscopy (STS). In Fig. 4, we plot $D(\omega)$ with the same parameters used in Fig. 3. For $m = -0.5$ with $\mathcal{N} = 2$, the resulting $D(\omega)$ has a finite value at $\omega = 0$. It has a peak at $\omega = 0$. Similar to this case, for $m = 0$ with $\mathcal{N} = 1$, LDOS has a peak structure at $\omega = 0$. On the other hand, for $m = 0.5$, LDOS has a gap structure where $D(\omega) = 0$ for $|\omega| < 0.25$. The absence of peak structure at $\omega = 0$ is consistent with $\mathcal{N} = 0$, where there is no chiral Majorana edge mode. The presence of the chiral Majorana edge mode seriously changes the resulting zero energy LDOS at the edge. Thus, it is possible to check the presence of chiral

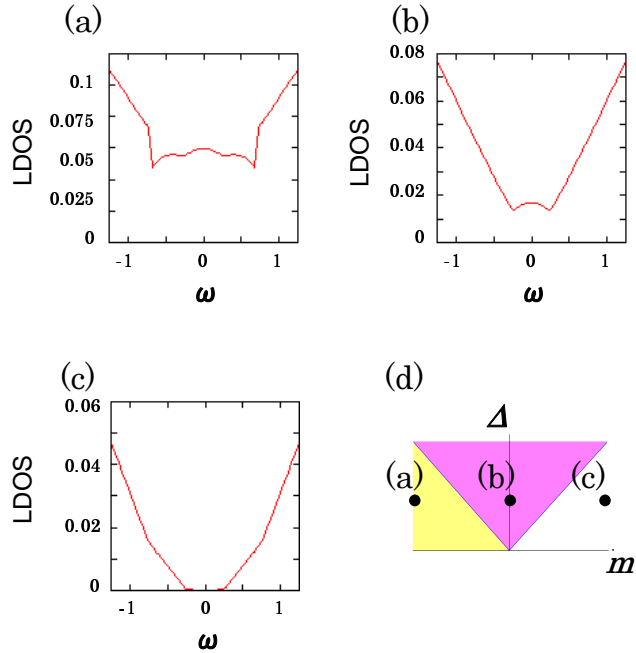


FIG. 4: (Color online) LDOS at the edge. (a) $m = -0.5$, (b) $m = 0$, and (c) $m = 0.5$. At these parameters, the gap of the bulk bands is 0.25 in all cases. For (a) and (b), there is no energy gap in LDOS.

Majorana edge modes by STS. However, there is no qualitative difference between $\mathcal{N} = 2$ and $\mathcal{N} = 1$ phases as seen from LDOS. From the discussion based on the Chern number, we can expect that there are degenerate two edge states in $\mathcal{N} = 2$ phase.

To discriminate $\mathcal{N} = 1$ phase from $\mathcal{N} = 2$ phase, we need a further idea: We apply the magnetic field to the system to make sure the difference between these two phases. We add the Zeeman term $\mu_B \mathbf{H} \cdot \boldsymbol{\sigma}$ in the original Hamiltonian, where μ_B is the Bohr magneton, \mathbf{H} is the Zeeman magnetic field. The magnitude of the bulk energy gap E_g is influenced by the Zeeman magnetic field, which is given by $E_g = |\sqrt{m^2 + (\mu_B \mathbf{H})^2} - \Delta|$. In Fig.5, $N(k_y, \omega)$ is plotted for $\Delta = 0.25$ and $\mu_B |\mathbf{H}| = 0.15$, where magnetic field is applied along the y direction. The resulting E_g is 0.27 and 0.1 for (a) $m = -0.5$ and (b) $m = 0$, respectively. As seen from Fig. 5(a), for $\mathcal{N} = 2$ phase, a splitting of the degenerate two chiral Majorana edge modes appears in the momentum resolved LDOS $N(k_y, \omega)$. On the other hand, for $\mathcal{N} = 1$ phase, single Majorana edge mode remains the same even in the presence of the magnetic field. Thus, we can discriminate $\mathcal{N} = 1$ and $\mathcal{N} = 2$ phase through the momentum resolved

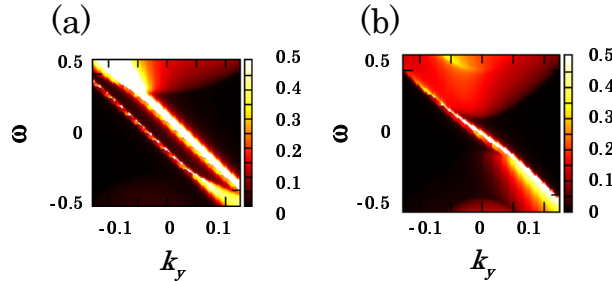


FIG. 5: (Color online) Momentum resolved LDOS at the edge $N(k_y, \omega)$ in the presence of magnetic field along the y -direction at $\Delta=0.25$ and $\mu_B|\mathbf{H}|=0.15$. (a): $m=-0.5$ and (b): $m=0$.

LDOS at the edge in the presence of Zeeman magnetic field. We also found that the splitting of Majorana edge modes for $\mathcal{N}=2$ phase appears only when the direction of the magnetic field is along the y direction. In order to understand the orientational dependence of the magnetic field on the energy spectrum, we introduce the winding number of the system at $k_y=0$ in the following subsection.

B. Winding number

The winding number W is one of the topological invariants that is well defined for the system with odd-number of spatial dimension [34]. It can count the number of zero energy state protected by topological property of the Hamiltonian. Although the dimension of our present system is two, if we fix k_y to a certain value, we can express the present system as an effective one-dimensional Hamiltonian [34]. In order to define W , we look for a hermitian matrix Γ which anti-commutes with the Hamiltonian;

$$\{H(\mathbf{k}), \Gamma\} = 0. \quad (11)$$

In the presence of the time reversal (TR) symmetry Θ , and particle-hole symmetry C , we can choose Γ as $\Gamma = -iC\Theta$. However, in the present system, the time reversal symmetry is broken by $m(\mathbf{p})$. Thus, we must find other Γ s. Since we found such Γ s only for $k_y = 0, \pi$, we focus on these cases in the following discussions. The searching of Γ is done as follows. Since Γ is a 4×4 hermitian matrix, it can be expressed by direct products of two Pauli matrices,

$$\Gamma_{\mu\nu} = \sigma_\mu \otimes \tau_\nu \quad (12)$$

where σ_μ ($\mu = 0, 1, 2, 3$) operates on the spin space, and τ_μ ($\mu = 0, 1, 2, 3$) on the particle-hole space. The suffix 0 indicates the unit matrix, and 1, 2 and 3 the x , y , and z components of the Pauli matrices, respectively. In a similar manner, the Hamiltonian can be expressed by the basis of $\Gamma_{\mu\nu}$. Then from the (anti-)commutation relations between the Pauli matrices, we find that only Γ_{23} and Γ_{32} anti-commute with the Hamiltonian. These matrices also anti-commute with the Hamiltonian even in the presence of Zeeman magnetic field along the z direction since the applied Zeeman term just changes the mass term in the Hamiltonian. On the other hand, if we apply the Zeeman magnetic field along the x -axis, only Γ_{23} anti-commutes with the Hamiltonian. Furthermore, if the direction of the applied magnetic field is the y -direction, only Γ_{32} anti-commutes. As is shown below, these differences imply that the topological nature of the Hamiltonian strongly depends on the direction of the Zeeman magnetic field.

Using these Γ s, we can define the winding number for each Γ . First, we diagonalize these Γ matrices;

$$U_\Gamma^\dagger \Gamma U_\Gamma = \begin{pmatrix} \mathbf{I}_{2 \times 2} & 0 \\ 0 & -\mathbf{I}_{2 \times 2} \end{pmatrix} \quad (13)$$

and transform the Hamiltonian to anti-diagonalized form by U_Γ .

$$U_\Gamma^\dagger H(\mathbf{k}) U_\Gamma = \begin{pmatrix} 0 & q(\mathbf{k}) \\ q(\mathbf{k})^\dagger & 0 \end{pmatrix}. \quad (14)$$

Then we calculate the determinant of the sub matrix $q(\mathbf{k})$ in Eq.(14), and denote its real part as m_1 and imaginary part as m_2 .

$$\det |q(\mathbf{k})| \equiv m_1(\mathbf{k}) + im_2(\mathbf{k}) \quad (15)$$

Finally, we obtain the winding number W as the following integral;

$$W = \frac{1}{2\pi} \int_{-\pi}^{\pi} \frac{\partial \theta(\mathbf{k})}{\partial k_x} \Bigg|_{k_y=0} dk_x \quad (16)$$

where

$$\theta(\mathbf{k}) \equiv \arg \det |q(\mathbf{k})| = \tan^{-1} \frac{m_2(\mathbf{k})}{m_1(\mathbf{k})}. \quad (17)$$

Here we only consider the winding number at $k_y = 0$ since they are found to be zero at $k_y = \pi$ in the following cases. We denote the winding number for Γ_{23} and Γ_{32} as W_{23} and

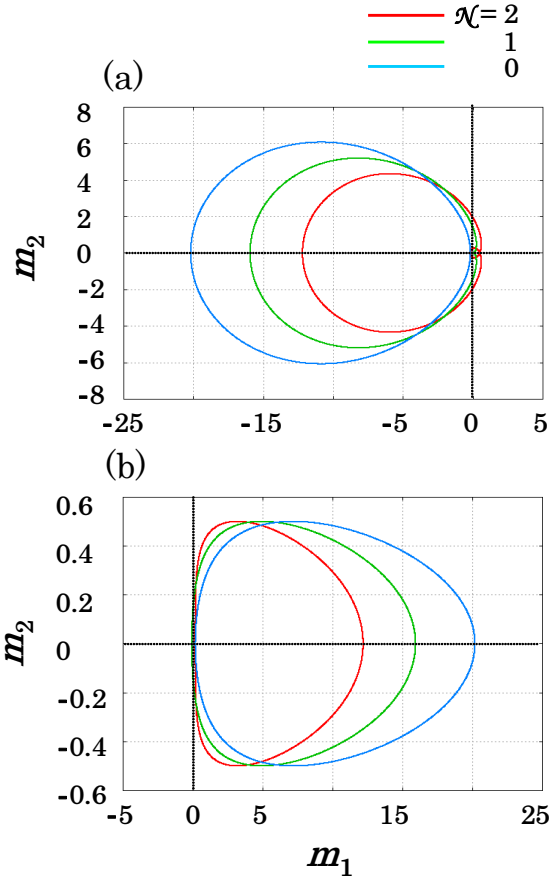


FIG. 6: (Color online) Contour plots of $m_1(\mathbf{k})$ and $m_2(\mathbf{k})$ for (a) W_{23} and (b) W_{32} . Here we fix k_y as $k_y = 0$ and changes k_x from $-\pi$ to π .

W_{32} , respectively. The winding numbers W_{23} and W_{32} become visible by plotting m_1 and m_2 in the first Brillouin zone as shown in Fig. 6. To make it clear, we enlarge the scale of Fig. 6 around the origin, in Fig. 7. The number of the rotation of the contour around the origin just corresponds to the winding number. The obtained W_{23} and W_{32} are summarized in Table I.

From the winding numbers in Table I, we can derive the following results. Let us first consider the case without the Zeeman magnetic field. In this case, both of W_{23} and W_{32} are well-defined. Then, the bulk-edge correspondence tells us that the number of zero energy states at $k_y = 0$ should be consistent with these winding numbers. As a result, there should be two zero energy edge states at $k_y = 0$ for $\mathcal{N} = 2$ phase, and one zero energy edge state for $\mathcal{N} = 1$. Here note that $W_{32} = 0$ for $\mathcal{N} = 2$ does not necessarily mean no zero energy

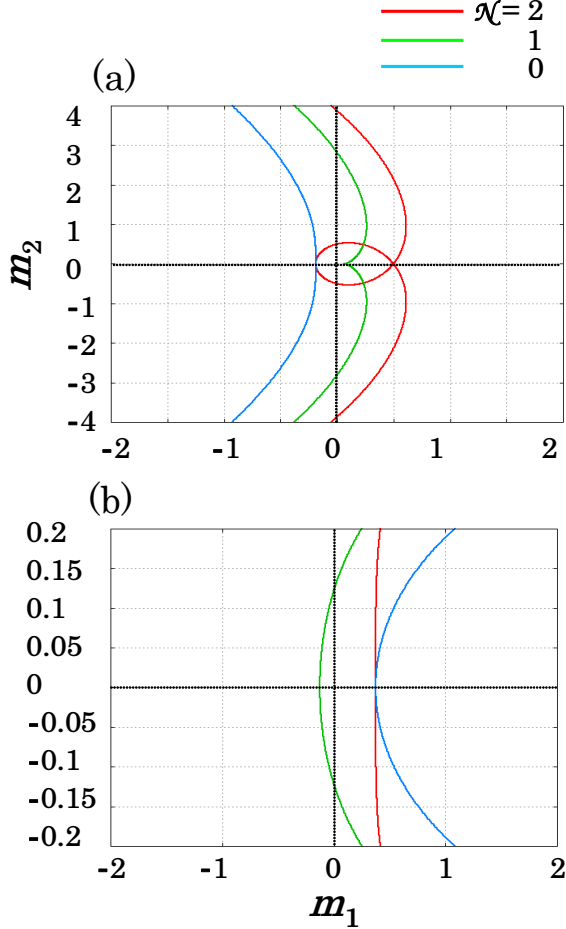


FIG. 7: (Color online) Enlarged plots of Fig. 6.

edge states at $k_y = 0$. To be consistent with $W_{23} = 2$ for $\mathcal{N} = 2$ at the same time, we need to have two zero energy edge states at $k_y = 0$. These two zero modes excellently agree with the two-fold degeneracy of the chiral Majorana edge modes found in Fig.3(a).

Now consider the case with a weak Zeeman magnetic field. As was mentioned above, W_{23} becomes ill-defined if we apply the Zeeman magnetic field in the y -direction. Thus, the number of the zero energy state at $k_y = 0$ is determined solely by W_{32} in this case. It is found that the remaining winding number W_{32} takes the same value as that without the Zeeman magnetic field, so for $\mathcal{N} = 2$ phase, the zero energy states at $k_y = 0$ should vanish. This result excellently agrees again with the lifting of the degeneracy of the chiral Majorana modes in Fig.5(a). These winding numbers also explains why the degeneracy is not lifted off if the Zeeman magnetic field is along the x or z -direction: In these cases, W_{23} remains

	$\mathcal{N} = 2$	$\mathcal{N} = 1$	$\mathcal{N} = 0$	$\mathbf{H} \parallel \hat{\mathbf{x}}$	$\mathbf{H} \parallel \hat{\mathbf{y}}$	$\mathbf{H} \parallel \hat{\mathbf{z}}$
W_{23}	2	1	0	○	×	○
W_{32}	0	1	0	×	○	○

TABLE I: Correspondence between the winding number W and the Chern number \mathcal{N} . We also show the validity of the winding numbers in the presence of the Zeeman magnetic field. W_{23} can not be defined for the applied magnetic field along y -direction, while W_{32} can not be defined for the applied magnetic field along the x -direction.

well-defined, so the two degenerate zero modes also remain at $k_y = 0$.

Finally, we discuss the edge state in $\mathcal{N} = 1$ phase. For any weak Zeeman magnetic field, at least one of W_{23} and W_{32} is well-defined, and both of them take 1. Thus, a single zero energy edge mode is always ensured at $k_y = 0$. In this sense, the edge state at $k_y = 0$ in $\mathcal{N}=1$ phase is 'robust' against perturbation.

C. edge state for finite μ

In this subsection, we consider $\mu \neq 0$ case, which corresponds to a doped QAHS case. It has been clarified that the condition for closing of the bulk band gap is as follows [29];

$$\Delta^2 + \mu^2 = m^2 \quad \text{when } \mu \neq 0. \quad (18)$$

The momentum resolved LDOS $N(k_y, \omega)$ is plotted in Figs. 8(a) and (b) for (a) $\mu = 0$ and (b) $\mu = 0.3$, respectively. (We set here $m = 0.3$ and $\Delta = 0.25$.) Since the magnitude of the bulk energy gap E_g is given by the minimum value of $E_g = |m + \sqrt{\mu^2 + \Delta^2}|$ and $E_g = |m - \sqrt{\mu^2 + \Delta^2}|$, the resulting E_g is 0.05 and 0.09 for (a) and (b), respectively. There is no chiral Majorana edge state in Fig. 8(a), but it exists in Fig. 8(b). Therefore, with the change of μ , the chiral Majorana edge state is generated. In other words, the change of μ introduces the quantum phase transition of the topological number from $\mathcal{N} = 0$ to $\mathcal{N} = 1$. Actually, the boundaries of the three phases (*i.e.* $\mathcal{N} = 0, 1, 2$) depend on the values of μ in addition to m and Δ . See Fig. 8(c).

Now, we focus on the edge state for $\mathcal{N} = 2$ with nonzero μ . In Fig. 9(a), the momentum resolved LDOS $\mathcal{N}(k_y, \omega)$ is plotted for $\mu = 0.2$, $\Delta = 0.25$ and $m = -0.3$. Since the

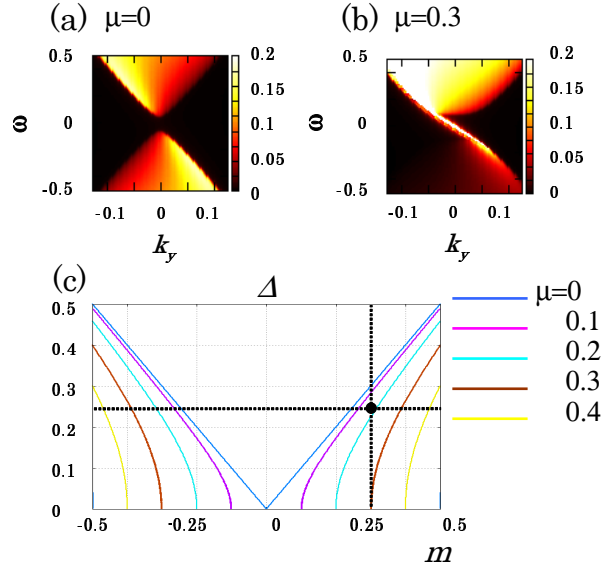


FIG. 8: (Color online) Energy spectrum of the edge modes are plotted as a function of k_y with $m=0.3$ and $\Delta=0.25$ for (a) $\mu = 0$, and (b) $\mu = 0.3$. (c)phase boundary of $\mathcal{N} = 2$, $\mathcal{N} = 1$, and $\mathcal{N} = 0$ phases are plotted as a function of Δ and m for various μ [29].

magnitude of the bulk energy gap E_g is expressed as

$$E_g = | \sqrt{m^2 + (\mu_B H)^2} - \sqrt{\mu^2 + \Delta^2} |$$

E_g is 0.18 in the present case. Comparing Fig. 9(a) with Fig.3(a), we find that the degenerate two Majorana edge modes realized in $\mathcal{N} = 2$ phase for $\mu = 0$ is lifted off by the doping.

If we change m from $m = -0.5$ to $m = 0$, with fixing $\mu = 0.2$ and $\Delta = 0.25$, the corresponding Chern number changes from $\mathcal{N} = 2$ to $\mathcal{N} = 1$. In Fig. 9(b), the momentum resolved LDOS $\mathcal{N}(k_y, \omega)$ is plotted, where E_g is given by 0.32. The chiral Majorana edge mode exists for $|\omega| < 0.32$. By contrast to the edge state of $\mathcal{N} = 2$, that of $\mathcal{N} = 1$ is robust against doping.

IV. SUMMARY

In this paper, we have studied the edge states of QAHS coupled with spin-singlet s -wave superconductor by the proximity effect. We have calculated the energy spectrum of the edge states and the resulting local density of states for various magnitudes of mass term

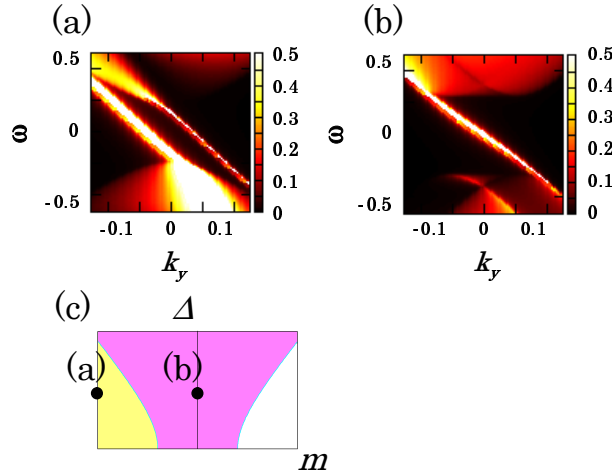


FIG. 9: (Color online) Energy spectrum of the edge modes are plotted as a function of k_y with $\mu=0.2$ and $\Delta=0.25$ for (a) $m = -0.5$, and (b) $m = 0$, respectively. (c) Schematic phase diagram for $\mu \neq 0$. The light yellow region corresponds to $\mathcal{N} = 2$, and the dark red one to $\mathcal{N} = 1$. The dots denotes the parameters corresponding to Figs.9(a) and (b).

m , pair potential Δ and chemical potential μ . The presence or absence of chiral Majorana edge modes influence seriously on the local density of state. We have clarified that it is possible to discriminate the state with nonzero Chern number \mathcal{N} from that with $\mathcal{N} = 0$ by observing local density of states by STS. Since chiral Majorana edge modes for $\mathcal{N} = 2$ are degenerate each other, it is difficult to discriminate $\mathcal{N} = 1$ and $\mathcal{N} = 2$ state by simply looking at the energy dispersion relation. To resolve this problem, we apply the Zeeman magnetic field. We find when the direction of the magnetic field is parallel to the interface, the degeneracy of the present two chiral Majorana edge modes in $\mathcal{N} = 2$ states are lifted off. Due to the presence of the bulk edge correspondence, the number of the chiral edge modes can be evaluated by the winding number defined at $k_y = 0$. For $\mathcal{N} = 1$ state, the resulting chiral Majorana edge mode are protected by the topological property of the bulk Hamiltonian.

Acknowledgment

We would like to express our sincere thanks to M. Oshikawa for giving meaningful advices to us. And this work was supported in part by the Grant-in Aid for Scientific Research from MEXT of Japan, "Topological Quantum Phenomena" No.22103005 (Y.T, M.S.),

- [1] L. J. Buchholtz and G. Zwicknagl, Phys. Rev. B **23**, 5788 (1981); J. Hara and K. Nagai, J. Hara and K. Nagai, Prog. Theor. Phys. **74**, 1237 (1986).
- [2] S. Kashiwaya and Y. Tanaka, Rep. Prog. Phys. **63**, 1641 (2000).
- [3] T. Löfwander, V. S. Shumeiko and G. Wendin, Supercond. Sci. Technol. **14**, R53 (2001),
- [4] C. R. Hu, Phys. Rev. Lett. **72**, 1526 (1994).
- [5] Y. Tanaka and S. Kashiwaya, Phys. Rev. Lett. **74**, 3451 (1995).
- [6] M. Matsumoto and M. Sigrist, J. Phys. Soc. Jpn. **68**, 994 (1999); C. Honerkamp and M. Sigrist, J. Low Temp. Phys. **111**, 895 (1998); M. Yamashiro, Y. Tanaka, and S. Kashiwaya, Phys. Rev. B **56**, 7847 (1997).
- [7] J. Goryo and K. Ishikawa, J. Phys. Soc. Jpn. **67**, 3006 (1998); A. Furusaki, M. Matsumoto, and M. Sigrist, Phys. Rev. B **64** 054514 (2001).
- [8] X.L. Qi, T. L. Hughes, S. Raghu and S.C. Zhang, Phys. Rev. Lett. **102**, 187001 (2009)
- [9] See for e.g., *The Quantum Hall effect*, edited by R.E. Prange and S.M. Girvin, (Springer-Verlag, 1987), and references therein.
- [10] D. J. Thouless, M. Kohmoto, M. P. Nightingale, and M. den Nijs, Phys. Rev. Lett. **49**, 405 (1982); M. Kohmoto, Ann. Phys. **160**, 343 (1985).
- [11] C. L. Kane and E. J. Mele, Phys. Rev. Lett. **95**, 146802 (2005); C. L. Kane and E. J. Mele, Phys. Rev. Lett. **95**, 226801 (2005); B. A. Bernevig, and S. C. Zhang, Phys. Rev. Lett. **96**, 106802 (2006); B. A. Bernevig, T. L. Hughes, and S. C. Zhang, Science **314** 1757 (2006); L. Fu and C. L. Kane, Phys. Rev. B **74**, 195312 (2006).
- [12] H. Z. Hasan and C. L. Kane, Rev. Mod. Phys. **82** 3045 (2010).
- [13] E. Bauer, G. Hilscher, H. Michor, Ch. Paul, E.W. Scheidt, A. Gribanov, Yu. Seropgin, H. Noël, M. Sigrist, and P. Rogl, Phys. Rev. Lett. **92**, 027003 (2004); K. Togano, P. Badica, Y. Nakamori, S. Orimo, H. Takeya, and K. Hirata, Phys. Rev. Lett. **93**, 247004 (2004); M. Nishiyama, Y. Inada, and G. Q. Zheng, Phys. Rev. B **71**, 220505(R) (2005); A. D. Hillier, J. Quintanilla, and R. Cywinski, Phys. Rev. Lett. **102**, 117007 (2009).
- [14] N. Reyren, S. Thiel S, A. D. Caviglia, L. F. Kourkoutis, G. Hammerl, C. Richter, C. W. Schneider, T. Kopp, A. S. Ruetschi, D. Jaccard, M. Gabay, D.A. Muller, J. M. Triscone, J.

Mannhart, Science **317**, 1196 (2007).

[15] M. Sato, Phys. Rev. B **73** 214502 (2006); M. Sato and S. Fujimoto, Phys. Rev. B **79**, 094504 (2009);

[16] Y. Tanaka, T. Yokoyama, A. V. Balatsky and N. Nagaosa, Phys. Rev. B **79**, 060505(R) (2009).

[17] T. Yokoyama, Y. Tanaka and J. Inoue, Phys. Rev. B **72** 220504(R) (2005); C. Inotakis, N. Hayashi, Y. Sawa, T. Yokoyama, U. May, Y. Tanaka, and M. Sigrist, Phys. Rev. B **76**, 012501 (2007); M. Eschrig, C. Inotakis, and Y. Tanaka, arXiv:1001.2486.

[18] A.B. Vorontsov, I. Vekhter, and M. Eschrig, Phys. Rev. Lett. **101**, 127003 (2008).

[19] C.K. Lu and S. Yip, Phys. Rev. B **80**, 024504 (2009).

[20] Y. Tanaka, Y. Mizuno, T. Yokoyama, K. Yada and M. Sato, Phys. Rev. Lett. **105**, 097002 (2010).

[21] K. Yada, M. Sato, Y. Tanaka and T. Yokoyama, Phys. Rev. B **83**, 064505 (2011).

[22] A. P. Schnyder, P. M. R. Brydon, D. Manske, and C. Timm, Phys. Rev. B **82**, 184508 (2010).

[23] A. P. Schnyder, S. Ryu, arXiv:1011.1438.

[24] R. Roy, arXiv:cond-mat/0608064. R. Roy, arXiv:0803.2881; M. Sato, Phys. Rev. B **79**, 214526 (2009); M. Sato, Phys. Rev. B **81**, 220504(R) (2010);

[25] A. P. Schnyder, S. Ryu, A. Furusaki, and A. W. W. Ludwig, Phys. Rev. B **78**, 195125 (2008), S. Ryu, A. P. Schnyder, A. Furusaki, A. Ludwig, New J. Phys. 12, 065010 (2010).

[26] Y. Maeno, H. Hashimoto, K. Yoshida, S. Nishizaki, T. Fujita, J. G. Bednorz, and F. Lichtenberg, Nature **372**, 532 (1994).

[27] L. Fu and C. L. Kane, Phys. Rev. Lett. **100**, 096407 (2008); L. Fu and C. L. Kane, Phys. Rev. Lett. **102**, 216403 (2009); A. R. Akhmerov, J. Nilsson, and C. W. J. Beenakker, Phys. Rev. Lett. **102**, 216404 (2009); Y. Tanaka, T. Yokoyama and N. Nagaosa, Phys. Rev. Lett. **103**, 107002 (2009).

[28] M. Sato, Y. Takahashi, and S. Fujimoto, Phys. Rev. Lett. **103**, 020401 (2009); M. Sato, Y. Takahashi and S. Fujimoto, Phys. Rev. B **82**, 134521 (2010); J. D. Sau, R. M. Lutchyn, S. Tewari, and S. Das Sarma, Phys. Rev. Lett. **104**, 040502 (2010); J. Alicea, Phys. Rev. B **81**, 125318 (2010).

[29] X. L. Qi, T. L. Hughes, and S. C. Zhang, Phys. Rev. B **82**, 184516 (2010); S. B. Chung, X. L. Qi, J. Maciejko, and S.C. Zhang, arXiv:1008.2003.

[30] X. L. Qi, Y. S. Wu, and S. C. Zhang, Phys. Rev. B **74**, 085308 (2006).

- [31] C. X. Liu, X. L. Qi, X. Dai, Z. Fang, and S. C. Zhang, Phys. Rev. Lett. **101**, 146802 (2008).
- [32] R. Yu, W. Zhang, H. Zhang, S. Zhang, X. Dai, and Z. Fang, Science **329**, 61 (2010).
- [33] M. Mastumoto and H. Shiba, J. Phys. Soc. Jpn. **64**, 5 (1995).
- [34] M. Sato, Y. Tanaka, K. Yada and T. Yokoyama, arXiv:1102.1322.